Vol. 12, No. 2 (2023) : 509 - 523
DOI : http://dx.doi.org/10.23960/jtep-l.v12i2.509-523
JURNAL TEKNIK PERTANIAN LAMPUNG
ISSN 2302-559X (print) / 2549-0818 (online)
Journal homepage : https://jurnal.fp.unila.ac.id/index.php/JTP

Zonation of Flood-Prone Areas Based on Remote Sensing Data and Hydrodynamic Models

Samsul Bachri[1] and Arif Faisol[2]✉

[1]Program Studi Ilmu Tanah, Fakultas Pertanian, Universitas Papua, Papua Barat. INDONESIA
[2]Program Studi Teknik Pertanian dan Biosistem, Fakultas Teknologi Pertanian, Universitas Papua, Papua Barat. INDONESIA

Article History :
Received : 14 October 2022
Received in revised form : 2 February 2023
Accepted : 8 February 2023

Keywords :
Climate Hazards Group Infrared Precipitation with Stations,
DEMNAS,
HEC-RAS,
Satellite Imagery,
Sentinel 2.

✉Corresponding Author:
arif.unipa@gmail.com

ABSTRACT

Many watersheds in Manokwari are classified as flood-prone areas with a frequency of more than 1 flood per year. Limited rain stations and climate stations make it difficult to the zoning of flood-prone areas. This study aims to utilize remote sensing data and hydrodynamic models to zone flood-prone areas in watersheds (DAS). The research was conducted in the Wosi Watershed - Manokwari Regency - West Papua Province. The data used in this research is DEMNAS topographic data, Climate Hazards Group Infrared Precipitation with Stations (CHIRPS) data acquired 1996 – 2020, Sentinel 2 imagery acquired 21 September 2020, and river maps. The peak flow in the Wosi watershed was analyzed using rational methods and flood hazard zoning was analyzed using HEC-RAS. The research showed that the Wosi River was not able to accommodate the peak flow at various return periods, consequently, the Wosi River had the potential for flooding every year. The results of this study are relevant to actual events, therefore remote sensing data and hydrodynamic models can be used to analyze peak flow and flood hazard zoning.

1. INTRODUCTION

Floods are natural disasters that dominate disaster events in Manokwari Regency. Based on data and information released by the National Disaster Management Agency (BNPB), in the period 2011 – 2020 floods in Manokwari Regency occurred every 1 – 2 years. Flood events in Manokwari Regency in the period 2011 – 2020 released by BNPB are presented in Table 1.

Table 1. Flood events in Manokwari Regency (BNPB, 2021)

Year	2011	2013	2014	2016	2018	2019	2020
Flood event	1	1	1	1	2	4	2

The Wosi watershed is one of the flood-prone areas in Manokwari Regency. Arifin *et al*. (2019) reported that the frequency of flood events in the Wosi watershed is very high with an occurrence frequency of more than 1 time in 1 year. This is due to the very low capacity of the Wosi River, namely ± 26.99 m^3/hour (Pamuji & Hardianti, 2019).

The government has issued several standards related to flood analysis and mapping of flood-sensitive areas, including the Indonesian National Standard (SNI) number 2415/2016 concerning Procedures for Calculation of Planned Flood Discharge (SNI, 2016) and SNI number 8197/2015 concerning Methods for Flood-Sensitive Mapping Scale 1:50,000 and 1:25,000 (SNI, 2015). Flood analysis and flood area mapping involve land physical parameters and climate parameters (SNI, 2016; 2015). The physical parameters of the land used in the flood analysis include topography, geology (rock type, physical properties of the rock, rock uniformity, soil texture, and structure), and land cover. While the climate parameter used in the flood analysis is rain (SNI, 2016; 2015).

Currently, physical parameters and climate parameters from remote sensing observations are available which can be used for flood analysis. Several physical and climate parameters resulting from remote sensing observations are presented in Table 2, Table 3, and Table 4.

Table 2. Topographic data from remote sensing observations (Mulder *et al*., 2011; Treuhaft, 2020; Badan Informasi Geospasial, 2018)

No	Topographical Data	Spatial Resolution
1	*Advanced Spaceborn Thermal Emission and Reflection Radiometer* (ASTER)	30 m
2	*Shuttle Radar Topography Mission (*SRTM)	30 m and 90 m
3	DEMNAS	8 m
4	CartoSat	10 m
5	*Light Detection and Ranging* (LiDAR)	1 m
6	*Interferometric Synthetic Aperture Radar* (IfSAR)	5 m
7	Sentinel – 1	5 m
8	Radarsat	1 m – 8 m
9	*Envisat Advanced Synthetic Aperture Radar* (Envisat ASAR)	25 m

Table 3. Remote sensing data from satellite observations to identify land cover (Department of the Interior U.S. Geological Survey, 2016; Abrams & Hook, 2003;European Space Agency, 2015; French Space Agency, 2012)

No	Satellite Image	Spatial Resolution	Temporal Resolution
1	MODIS	250 m	Daily
2	ASTER	15 m	16 day
3	Landsat 8	15 m	15 day
4	Sentinel 2	10 m	10 day
5	Pléiades	0.5 m	Daily
6	IKONOS	0.82 m	3 day
7	OrbView-3	1 m	3 day
8	Quickbird	0.61 m	1 – 3.5 day
9	SPOT	2.50 m	2 – 3 day
10	GeoEye-1	0.41 m	3 day

Hydrodynamic models have been used extensively for flood modeling. Hydrodynamic models use the laws of physics to describe and replicate the movement of water and floods. Several hydrodynamic models commonly used in simulating water movement and flooding are presented in Table 5.

Table 4. Rainfall data from satellite observation (National Center for Atmospheric Research Staff, 2020)

No	Rainfall data	Spatial Resolution	Temporal Resolution
1	APHRODITE	~28 km	Daily
2	CHELSA	~1 km	Monthly
3	CHOMPS	~28 km	Daily
4	CMAP	~278 km	Monthly
5	CMORPH	~28 km	Daily
6	CPC	~56 km	Daily
7	CRU	~56 km	Monthly
8	GPCC	~56 km	Daily, Monthly
9	GPCP	~111 km	Daily
10	HOAPS	~56 km	Daily, Monthly
11	PERSIANN	~28 km	Daily
12	PREC/L	~278 km	Monthly
13	TerraClimate	~4 km	Monthly
14	TRMM	~28 km	4 hour, Daily, Monthly
15	GPM	~10 km	4 hour, Daily, Monthly
16	CHIRPS	~5 km	Daily, Monthly

Table 5. Hydrodynamic models for flood analysis

No	Hydrodynamic models	Developer
1	MIKE	Danish Hydraulic Institute (DHI)
2	HEC-RAS	U.S. Army Corps of Engineers
3	LISFLOOD-FP	Paul Bates – University of Bristol
4	TELEMAC-2D	Consortium: Electricite de France, Sogreah, Hydraulic Research Wallingford, Centre d'etudes Techniques Maritimes et Fluviales, Bundesanstalt fur Wasserbau, and Daresbury Lab.
5	TuFlow	BMT - Australia
6	Aquatic Ecosystem Model 3D (AEM3D)	Hydronumeric - Australia
7	Geophysical Fluid Dynamics Laboratory (GFDL)	National Oceanic and Atmospheric Administration (NOAA)
8	Princeton ocean model (POM)	Universitas Princeton – Amerika Serikat
9	Environmental Fluid Dynamic Code (EFDC)	Environmental Protection Agency (EPA) – Amerika Serikat
10	Packery Channel Hydrodynamic Model (PCH-Model)	Conrad Blucher Institute for Surveying and Science (CBI)
11	Coastal Modelling System (CMS)	U.S. Army Corps of Engineers
12	Finite Volume Coastal Ocean Model (FVCOM)	Marine Ecosystem Dynamic Modelling Laboratory

Several researchers around the world have used remote sensing data and hydrodynamic models to model and zoning flood-prone areas. Sing *et al*. (2020) used Cartosat and MIKE data to identify flood vulnerability zones in the Damodar – East India watershed. Giustarini *et al*. (2015) conducted flood hazard mapping on the Severn river – England using LISFLOOD-FP and Envisat ASAR data. Kareem *et al*. (2011) used MIKE and SRTM data to estimate flood inundation in the Fitzroy River – Australia. Alivio *et al*. (2019) used IFSAR and HEC-RAS data for zoning flood-sensitive areas in Kalilangan - the Philippines. Pietroniro *et al*. (2001) mapped the flood depths of Lake Mamawi and Lake Claire in Canada using hydrodynamic models and data from Radarsat, Landsat, and SPOT. Besides that, Tiwari *et al*. (2020) used Sentinel – 1, Sentinel – 2, and CHIRPS data to map flood inundation in Kerala – India. Narulita & Ningrum (2018) used CHIRPS data to analyze flood events in Indonesia. Yu *et al*. (2020) monitored flooding in the Songhua Watershed - China using CHIRPS data and MODIS satellite imagery. Yoshimoto & Amarnath (2017) utilized TRMM and PERSIANN data to model and predict flood inundation in the Mundeni Aru Watershed - Sri Lanka. Furthermore, Faisol *et al*. (2020) use GPM data to map the potential for flooding in Manokwari District - West Papua Province.

These studies show that the use of remote sensing data and hydrodynamic models have good accuracy in describing flood inundation and zoning of flood-sensitive areas (Alivio *et al*., 2019; Tiwari *et al*., 2020; Yoshimot & Amarnath, 2017). Based on these conditions, this study aims to utilize remote sensing data and hydrodynamic models for zoning flood-sensitive areas in the Wosi Watershed, Manokwari Regency, West Papua Province.

2. MATERIALS AND METHODS

This research was conducted in the Wosi Watershed (DAS), Manokwari Regency, West Papua Province. The research location was shown in Figure 1. The research steps were showed in Figure 2.

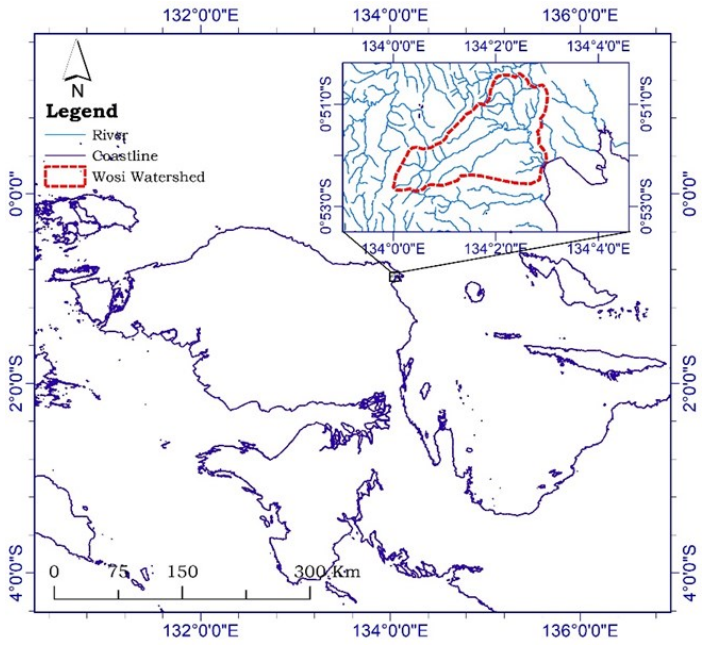

Figure 1. Research location

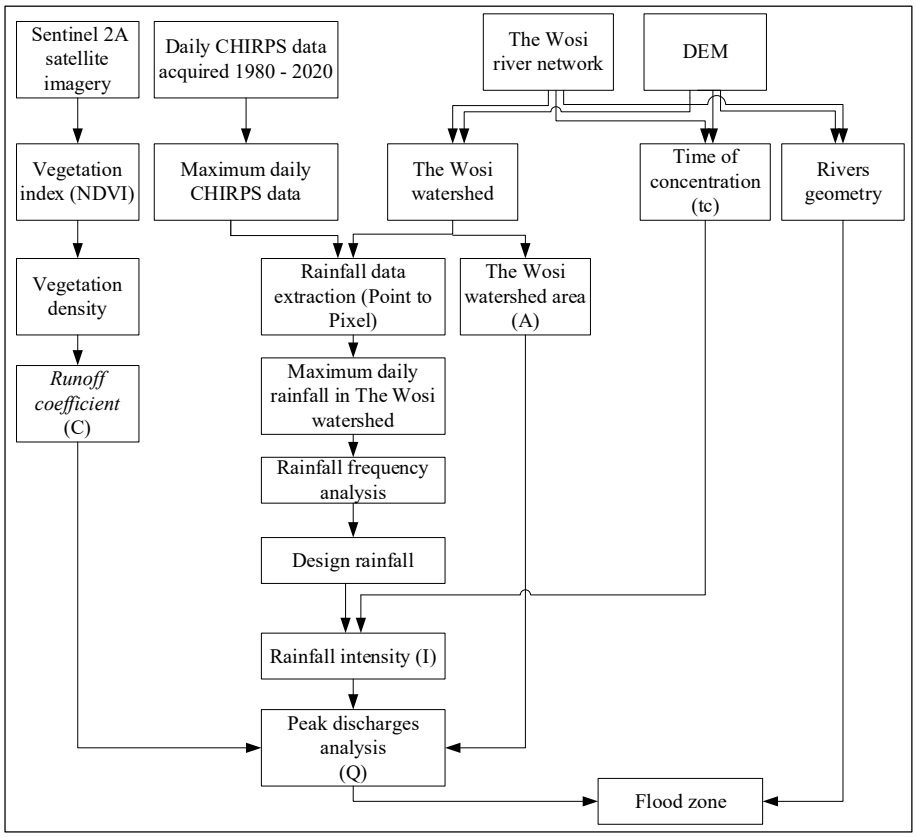

Figure 2. Flowchart of research

In general, this research consisted of 4 (four) main stages, namely; data inventory, rain data extraction, data analysis, and zoning of flood-sensitive areas. The data inventory aimed to collect DEMNAS data, CHIRPS data recorded from 1996 to 2020, Sentinel 2 satellite imagery recorded on 21 September 2020, and river network maps. Rain data extraction aimed to extract CHIRPS maximum daily rainfall data based on the Wosi watershed location using the point-to-pixel method. Rain data extraction was done manually by recording the maximum daily rainfall data from satellite observations at the watershed location or done automatically using geographic information system software. Data analysis aimed to analyze design rainfall and design discharge at various return periods, namely; 1 year, 2 years, 5 years, 10 years, 25 years, 50 years, and 100 years. Zonation of flood-prone areas aimed to map flood inundation using a hydrodynamic model.

The design discharge analysis was carried out using the rational method. This was because the Wosi watershed has an area of ± 13.07 km2. Based on the SNI (2016) the Rational method was used to analyze floods in a watershed area of up to 5,000 Ha or 50 km^2. Discharge analysis based on the Rational method was calculated using the following equation (Bedient *et al*., 2013; Eslamian, 2014; Mimikou *et al*., 2016; Ebissa, 2017):

$$Q = \frac{C_f C\ I\ A}{360} \quad (1)$$

where Q is the design discharge (m^3/second), C_f is the adjustment factor (correction) of the runoff coefficient, C is the runoff coefficient, I is the intensity of rainfall at the time

of concentration (mm/h), and *A* is the area of the watershed (ha). The adjustment factor (C_f) for each return period was presented in Table 6.

Table 6. Adjustment factor (C_f) of the runoff coefficient (Eslamian, 2014; Mimikou *et al*., 2016)

No	Return period (T) (year)	Adjustment factor (C_f)
1	1	1.00
2	2	1.00
3	5	1.00
4	10	1.00
5	25	1.10
6	50	1.20
7	100	1.25

The coefficient of rainwater runoff (*C*) was calculated using the plant density approach with the following equation (Suhardi *et al*., 2020; Suhardi & Entin, 2019):

$$C = 1 - \frac{VD}{100} \quad (2)$$

where *C* is the coefficient of rainwater runoff, and VD is the plant density.

Plant density was estimated using the following equation (Suhardi *et al*., 2020):

$$VD = 37{,}705\ NDVI - 1{,}596 \quad (3)$$

where VD is plant density, and NDVI is the Normalized Difference Vegetation Index or normalized vegetation index.

NDVI is calculated using the following equation (Liu & Mason, 2009):

$$NDVI = \frac{\rho_{NIR} - \rho_{RED}}{\rho_{NIR} + \rho_{RED}} \quad (4)$$

where NDVI is the Normalized Difference Vegetation Index, ρNIR is the near-infrared reflectance band value, and ρRED is the red band reflectance value.

Meanwhile, the NDVI of Sentinel 2 satellite images is calculated using the following equation (The European Space Agency, 2018):

$$NDVI = \frac{\rho_8 - \rho_4}{\rho_8 + \rho_4} \quad (5)$$

where ρ_8 is the reflectance band 8, and ρ_4 is the reflectance band 4.

Rainfall intensity (I) is calculated using the following Monobe equation (Kamiana, 2011; National Standardization Agency, 2016; Saputra *et al*., 2018; Sofia & Nursila, 2019):

$$I = \frac{R_{24}}{24}\left(\frac{24}{t_c}\right)^{\frac{2}{3}} \quad (6)$$

where I is the intensity of rainfall at the time of concentration (mm/h), R_{24} of the designed rainfall (mm), and t_c is the time of concentration (h).

The designed rainfall (R24) was analyzed using the normal distribution with the following equation:

$$R_{24} = \mu + K_t \sigma \quad (7)$$

where R_{24} is the design rainfall at the *t*-year return period, σ is the standard deviation (standard deviation) value of the maximum daily rainfall, μ is the average maximum daily rainfall value, and K_t is the reduction variable. The reducing variable (K_t) for each return period was presented in Table 7.

Table 7. Reducing variable (K_t) in the Normal Distribution

Return Period (T)	Probability (P)	Reducing variables (K_T)
year		
1.00	0.99	-3.05
1.25	0.80	-0.84
1.67	0.60	-0.25
2.00	0.50	0
2.50	0.40	0.25
5	0.20	0.84
10	0.10	1.28
20	0.05	1.64
50	0.02	2.05
100	0.01	2.33

Concentration time (t_c) is the time required for rainwater to flow from the farthest point to the outlet. Concentration time was calculated using the following Kirpich equation (BSN, 2016; Thompson, 2006; Hingray *et al*., 2015; Mimikou *et al*., 2016):

$$t_c = 0{,}01947\ L^{0{,}77}\ S^{-0{,}385} \quad (8)$$

where *tc* is the concentration-time (min), *L* is the length of the main river (m), and *S* is the slope of the main river. The main river slope (*S*) was calculated using the following equation (Mimikou *et al*., 2016):

$$S = \frac{H}{L} \quad (9)$$

where H is the elevation difference (height) on the main river, namely the difference in elevation between the farthest point and the outlet (m).

Zonation of flood-sensitive areas was analyzed using the HEC-RAS software. HEC–RAS uses the energy equation as a basis for analysis. The energy equation used is as follows (US Army Corps of Engineers, 2016):

$$Z_2 + Y_2 + \alpha_2 \frac{V_2^2}{2g} = Z_1 + Y_1 + \alpha_1 \frac{V_1^2}{2g} + h_e \quad (10)$$

where Y_1 and Y_2 are the depth of water at sections 1 and 2 (m); Z_1 and Z_2 are riverbed height from datum (m); V_1 and V_2 are average speed over the channel cross-section (m/s); α_1 and α_2 are speed coefficient; g is earth gravitation coefficient (m/s^2); and h_e is high energy loss (m).

3. RESULTS AND DISCUSSION

Based on the interpretation of CHIRPS data, the maximum daily rainfall in the Wosi watershed in the period 1996 – 2020 is 32 mm – 73 mm with an average (μ) of 53.07 mm, a standard deviation (σ) of 12.35 mm, and evenly distributed normally with a skewness coefficient (α) of 0.076. The maximum daily rainfall and the distribution of rain data in the Wosi watershed estimated by CHIRPS data are presented in Figure 3 and Figure 4.

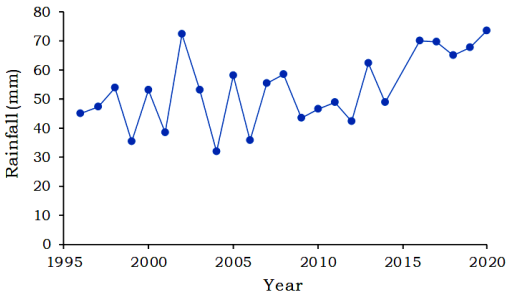

Figure 3. Maximum daily rainfall in the Wosi watershed

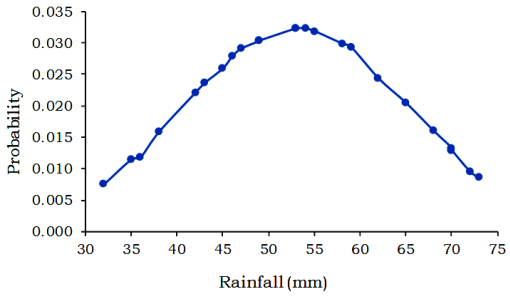

Figure 4. Distribution of maximum daily rainfall data in the Wosi watershed

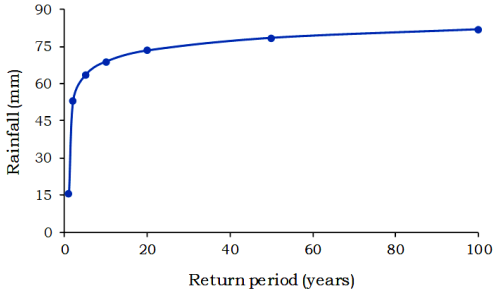

Figure 5. Graph of the design rainfall for the Wosi watershed at various return periods

Design rainfall in the Wosi watershed is 15 mm in the 1-year return period, 53 mm in the 2-year return period, and 63 mm in the 5-year return period. The design rainfall for the Wosi watershed for a return period of 1 year to 100 years based on CHIRPS data analysis and the normal distribution method is presented in Figure 5.

From the interpretation of DEMNAS topographic data and river network maps, the length of the main river in the Wosi watershed is ± 8.43 km and the slope of the main river is ± 0.038. The Wosi watershed topographic map is presented in Figure 6.

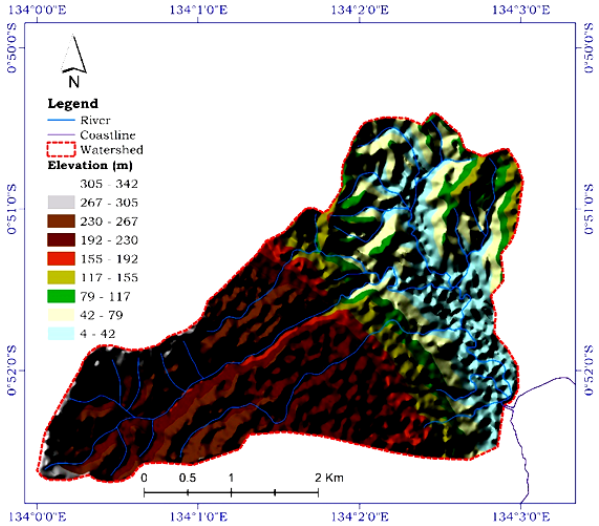

Figure 6. Topographic map of the Wosi watershed

Based on the interpretation of Sentinel 2 imagery, the NDVI value in the Wosi watershed is in the range of -0.16 to 0.86. While the value of the coefficient of rainwater runoff is in the range of 0.69 – 0.99 with an average value of 0.75. The Sentinel 2 image recorded on September 21, 2020 is presented in Figure 7. Meanwhile, the NDVI values and the water runoff coefficient in the Wosi DAS are presented in Figure 8, Figure 9, and Figure 10.

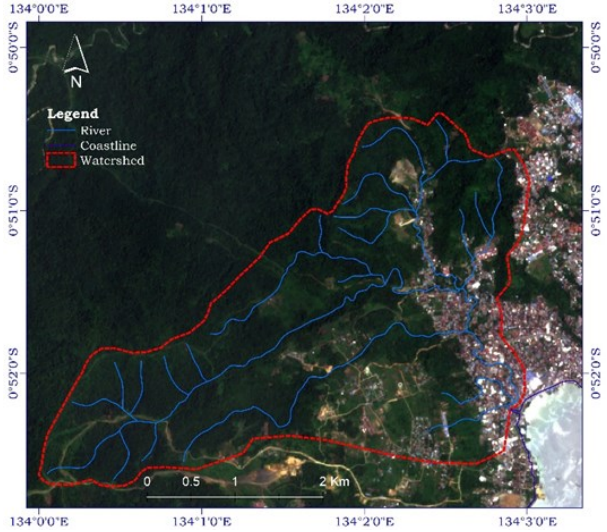

Figure 7. Sentinel 2 satellite imagery recorded on 21 September 2020

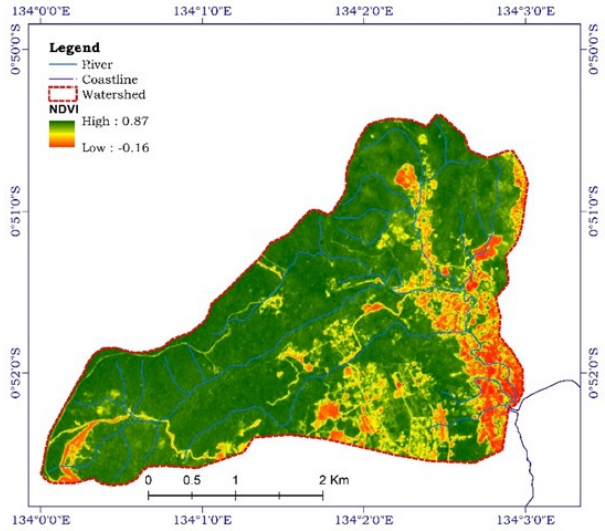

Figure 8. NDVI values in the Wosi watershed

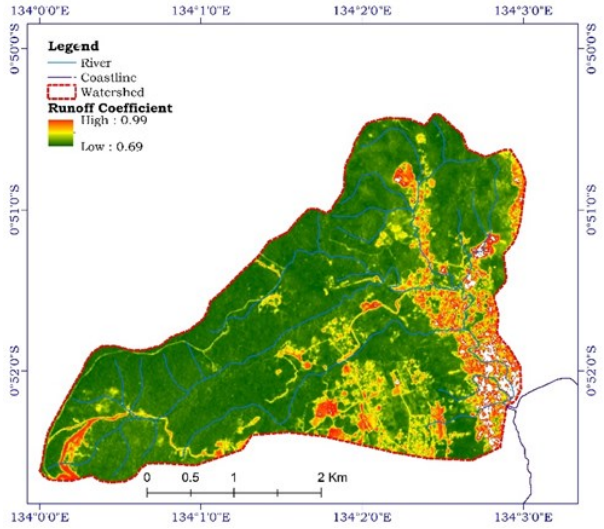

Figure 9. Distribution of rainwater runoff coefficients in the Wosi watershed

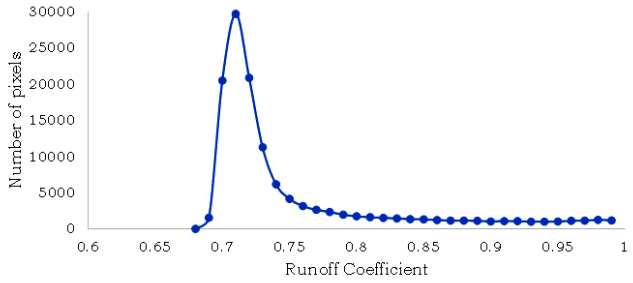

Figure 10. Graph of runoff coefficient in the Wosi watershed

The intensity of rainfall in the Wosi watershed based on the characteristics of the watershed is 5 mm/h for a 1-year design rainfall, 16 mm/h for a 2-year design rainfall, and 19 mm/h for a 5-year design rainfall. Rainfall intensity in the Wosi watershed for return periods of 1 year to 100 years is presented in Figure 11.

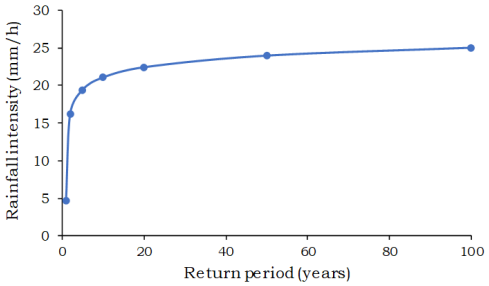

Figure 11. Rainfall intensity in the Wosi watershed at various return periods

The water discharge entering the Wosi River is estimated at 12.83 m3/second for a 1-year return period, 44.18 m3/second for a 2-year return period, and 52.81 m3/second for a 5-year return period. The design discharge in the Wosi watershed for the return period of 1 year to 100 years is presented in Figure 12.

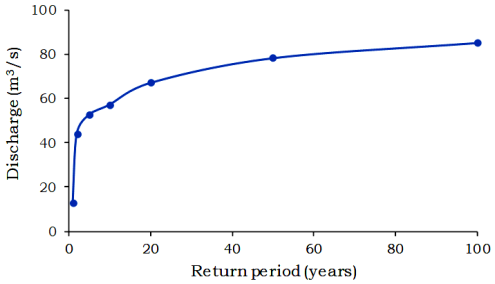

Figure 12. Graph of the Wosi watershed designed to discharge at various return periods

Based on the results of hydrodynamic analysis using HEC-RAS, the Wosi River is unable to accommodate the design discharge at various return periods, so it has the potential to flood every year. The results of the flood analysis in the Wosi watershed based on the hydrodynamic model are presented in Figure 13 to Figure 15. In the 1-year return period (Figure 13) the area that has the potential to be flooded is ± 17.56 ha, in the 2-year return period (Figure 14) the area that has the potential to be flooded ± 22.61 ha, and ± 23.89 ha at the 5 year return period (Figure 15). The overlay of flood inundation in the Wosi watershed at a return period of 1 to 5 years is presented in Figure 16.

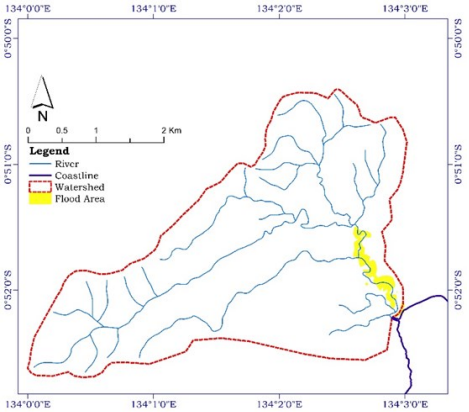

Figure 13. Flood inundation map of the Wosi watershed at 1 year return period

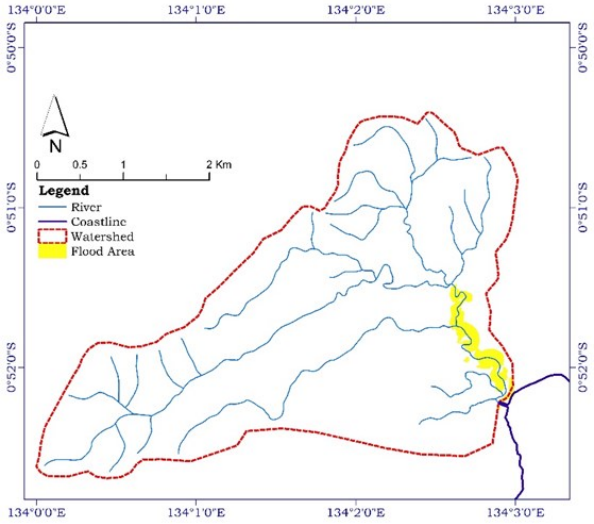

Figure 14. Flood inundation map of the Wosi watershed at 2 year return period

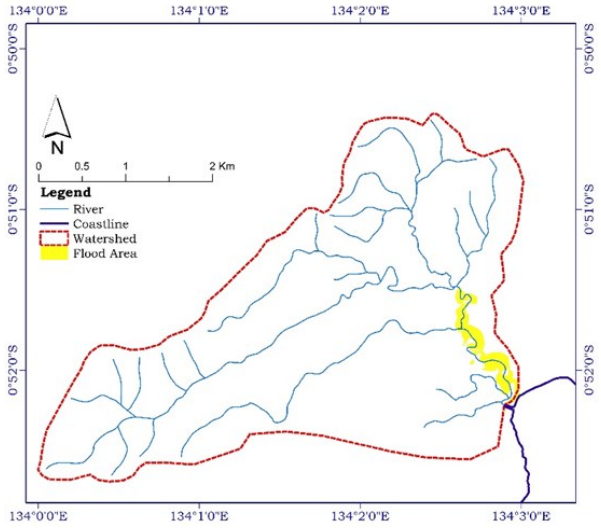

Figure 15. Map of the flood inundation of the Wosi watershed at the 5-year return period

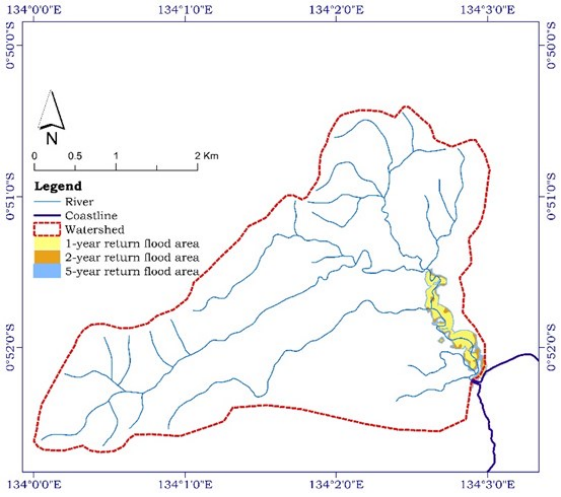

Figure 16. Flood inundation map of the Wosi watershed at a return period of 1 to 5 years

The results of this study are relevant to research conducted by Pamuji & Hardianti (Pamuji & Hardianti, 2019) that the capacity of the Wosi River is very low, namely 26.99 m3/hour so the Wosi River will not be able to accommodate the design discharge in the 1 year return period. Besides that, the results of this study are also relevant to the results of research conducted by Arifin *et al.* (2019) who reported that the frequency of flood events in the Wosi watershed is more than 1 time in 1 year.

4. CONCLUSIONS AND SUGGESTIONS

Based on the analysis of remote sensing data and hydrodynamic models, the Wosi River is unable to accommodate the design discharge at various return periods. In the 1 -year return period the area that could potentially be flooded was ± 17.56 ha, in the 2-year return period the area that was potentially inundated was ± 22.61 ha, and ± 23.89 ha in the 5-year return period. This is relevant to several studies which state that the capacity of the Wosi River is very low and it experiences flooding every year. So that remote sensing data and hydrodynamic models can identify and map flood-affected areas very well compared to actual events. However, the results of this study still need to be validated by ground checks in flood-affected areas.

REFERENCES

Abrams, M., & Hook, S. (2003). *ASTER User Handbook*. Jet Population Library.

Alivio, M. B. T., Puno, G. R., & Talisay, B. A. M. (2019). Flood Hazard Zones using 2d Hydrodynamic Modeling and Remote Sensing Approaches. *Global Journal of Environmental Science and Management*, ***5***(1), 1–16. https://doi.org/10.22034/gjesm.2019.01.01

Arifin, H., Heatubun, C. D., & Wahyudi, W. (2019). Analisis kawasan hutan dan tutupan hutan pada tiga daerah aliran sungai di Kabupaten Manokwari. *Cassowary*, ***2***(1), 49–67. https://doi.org/10.30862/casssowary.cs.v2.i1.22

Badan Informasi Geospasial. (2018). *DEMNAS✕ Seamless Digital Elevation Model (DEM) dan Batimetri Nasional*. https://tanahair.indonesia.go.id/demnas/#/.

Badan Nasional Penanggulangan Bencana. (2021). *Geoportal Kebencanaan Indonesia*. https://gis.bnpb.go.id/

Badan Standardisasi Nasional. (2015). *Metode Pemetaan Rawan Banjir Skala 1:50.000 dan 1:25.000* (1st ed.). Badan Standardisasi Nasional.

Badan Standardisasi Nasional. (2016). *SNI 2415: 2016 - Tata Cara Perhitungan Debit Banjir Rencana*.

Bedient, P. B., Huber, W. C., & Vieux, B. E. (2013). *Hydrology and Floodplain Analysis* (5th ed.). Pearson Education.

Department of the Interior U.S. Geological Survey. (2016). *Landsat 8 (L8) Data User Handbook* (2nd ed.). U.S. Geological Survey.

Ebissa, G. K. (2017). Hydrological Analysis and Peak Discharge Determination. *Journal of Mechanical and Civil Engineering*, ***14***(3), 33–48. https://doi.org/10.9790/1684-1403053348

Eslamian, S. (Ed.). (2014). *Engineering Hydrology* (1st ed.). CRC Press.

European Space Agency. (2015). *SENTINEL-2 User Handbook* (Issue 1). European Space Agency.

French Space Agency. (2012). *Pléiades Imagery User Guide* (2nd ed., Issue October). Astrium.

Giustarini, L., Chini, M., Hostache, R., Pappenberger, F., & Matgen, P. (2015). Flood Hazard Mapping Combining Hydrodynamic Modeling and Multi Annual Remote Sensing Data. *Remote Sensing*, ***7***(10), 14200–14226. https://doi.org/10.3390/rs71014200

Hingray, B., Picouet, C. P., & Musy, A. (2015). *Hydrology: a Science for Engineers* (1st ed.). CRC Press.

Kamiana, I. M. (2011). *Teknik Perhitungan Debit Rencana Bangunan Air* (1st ed.). Graha Ilmu.

Karim, F., Petheram, C., Marvanek, S., Ticehurst, C., Wallace, J., & Gouweleeuw, B. (2011). The Use of Hydrodynamic Modelling and Remote Sensing to Estimate Floodplain Inundation and Flood Discharge in a Large Tropical Catchment. *MODSIM 2011 - 19th International Congress on Modelling and Simulation - Sustaining Our Future: Understanding and Living with Uncertainty*, *October 2015*, 3796–3802.

Liu, J. G., & Mason, P. J. (2009). *Essential Image Processing and GIS for Remote Sensing* (1st ed.). Wiley & Sons, Ltd.

Mimikou, M. A., Baltas, E. A., & Tsihrintzis, V. A. (2016). *Hydrology and Water Resource System Analysis* (1st ed.). CRC Press.

Mulder, V.L., De Bruin, S., Schaepman, M.E., & Mayr, T.R. (2011). The use of remote sensing in soil and terrain mapping — A review. *Geoderma*, ***16***(2), 1-19. doi: 10.1016/j.geoderma.2010.12.018.

Narulita, I., & Ningrum, W. (2018). Extreme Flood Event Analysis in Indonesia Based on Rainfall Intensity and Recharge Capacity. *IOP Conference Series: Earth and Environmental Science*, ***118***(1). https://doi.org/10.1088/1755-1315/118/1/012045

National Center for Atmospheric Research Staff. (2020). *The Climate Data Guide: Precipitation Data Sets: Overview & Comparison table*. Agustus. https://climatedataguide.ucar.edu/climate-data/precipitation-data-sets-overview-comparison-table

Pamuji, K. E., & Hardianti, H. (2019). Evaluasi Hidrologi Daerah Aliran Sungai Wosi Dalam Menghadapi Curah Hujan Ekstrim. *Jurnal Natural*, ***15***(2), 67–77. https://doi.org/10.30862/jn.v15i2

Pietroniro, A., Leconte, R., Peters, D. L., & Prowse, T. D. (2001). Application of a hydrodynamic model in a freshwater delta using remote sensing. *Remote Sensing and Hydrology*, ***267***, 519–525.

Saputra, M., Fatimah, E., & Azmeri. (2018). Analisis Kapasitas Tampung dan Penentuan Kerusakan Sungai Aih Tripe Kabupaten Gayo Lues. *Jurnal Teknik Sipil*, ***1***(4), 915–928.

Singh, R. K., Kumar Villuri, V. G., Pasupuleti, S., & Nune, R. (2020). Hydrodynamic Modeling for Identifying Flood Vulnerability Zones in Lower Damodar River of Eastern India. *Ain Shams Engineering Journal*, ***11***(4), 1035–1046. https://doi.org/10.1016/j.asej.2020.01.011

Sofia, D. A., & Nursila, N. (2019). Analisis Intensitas , Durasi , dan Frekuensi Kejadian Hujan di Wilayah Sukabumi. *Jurnal Teknologi Rekayasa*, ***4***(1), 85–92. https://doi.org/10.31544/jtera.v4.i1.2019.85-92

Suhardi, G., & Entin. (2019). Estimation of Runoff Coefficient Using Satellite Imagery in Welang Watershed Pasuruan District Indonesia. *International Journal of Civil Engineering and Technology*, ***10***(6), 155–162. http://www.iaeme.com/IJCIET/index.asp155http://www.iaeme.com/ijciet/issues.asp JType=IJCIET&VType=10&IType=6

Suhardi, Hidayah, E., & Halik, G. (2020). Flash flood modeling using the artificial neural network (Case study: Welang Watershed, Pasuruan District, Indonesia. *IOP Conference Series: Earth and Environmental Science*, ***419***(1). https://doi.org/10.1088/1755-1315/419/1/012123

The European Space Agency. (2018). *Level-2A Algorithm Overview*. https://sentinels.copernicus.eu/web/sentinel/technical-guides/sentinel-2-msi/level-2a/algorithm

Thompson, D. B. (2006). *The Rational Method, Regional Regression Equations, and Site-Specific Flood-Frequency Relations*.

Tiwari, V., Kumar, V., Matin, M. A., Thapa, A., Ellenburg, W. L., Gupta, N., & Thapa, S. (2020). Flood Inundation Mapping- Kerala 2018 ; Harnessing the Power of SAR , Automatic Threshold Detection Method and Google Earth Engine. *Plos One*, ***15***(8), 1–17. https://doi.org/10.1371/journal.pone.0237324

Treuhaft, R. (2020). *Instrument Shuttle Radar Topography Mission*. Jet Propulsion Laboratory. https://www2.jpl.nasa.gov/srtm/instrumentinterfmore.html

US Army Corps of Engineers. (2016). HEC-RAS River Analysis System : Hydraulic Reference Manual Version 5.0. In *Hydrologic Engineering Center* (1st ed., Issue February). Hydrologic Engineering Center.

Yoshimot, S., & Amarnath, G. (2017). Applications of satellite-based rainfall estimates in flood inundation modeling-A case study in Mundeni Aru River Basin, Sri Lanka. *Remote Sensing*, ***9***(10). https://doi.org/10.3390/rs9100998

Yu, C., Hu, D., Zhang, Y., Liu, M., & Wang, S. (2020). Rainfall-runoff Simulation and Flood Dynamic Monitoring based on CHIRPS and MODIS-ET. *International Journal of Remote Sensing*, ***41***(11), 4206–4225. https://doi.org/https://doi.org/10.1080/01431161.2020.1714779